JGR Space Physics

RESEARCH ARTICLE
10.1029/2024JA033382

Effects of Fine Spectral Structure of Chorus Emissions on Nonlinear Scattering and Acceleration of Radiation Belt Electrons

Miroslav Hanzelka[1,2], Yuri Shprits[1,3,4], Dedong Wang[1], Bernhard Haas[1,3], Ondřej Santolík[2,5], and Longzhi Gan[6]

[1]GFZ German Research Centre for Geosciences, Potsdam, Germany, [2]Institute of Atmospheric Physics of the Czech Academy of Sciences, Prague, Czech Republic, [3]Institute of Physics and Astronomy, University of Potsdam, Potsdam, Germany, [4]Department of Earth, Planetary, and Space Sciences, University of California, Los Angeles, CA, USA, [5]Faculty of Mathematics and Physics, Charles University, Prague, Czech Republic, [6]Center for Space Physics, Boston University, Boston, MA, USA

Abstract Whistler-mode chorus waves play a crucial role in accelerating electrons in Earth's outer radiation belt to relativistic and ultrarelativistic energies. While this electron evolution is typically modeled using a diffusion approximation for scattering, high-amplitude chorus waves induce nonlinear resonant effects that challenge this approach on short time scales. The long-term influence of these nonlinear interactions on radiation belt dynamics remains an unresolved issue. Recent simplified models suggest rapid nonlinear acceleration to ultrarelativistic energies, with formation of butterfly distributions during parallel wave propagation. In this study, we introduce a novel numerical approach based on Liouville phase space density mapping to investigate nonlinear scattering by high-amplitude waves over extended periods (minutes and beyond). We use a numerical wave field model of lower-band chorus risers that includes realistic fine-spectral features including subpacket modulations, phase decoherence, and jumps in wave normal angle. By incorporating these detailed spectral characteristics of the waves, we demonstrate that the rapid acceleration occurs across a broader pitch-angle range, forming a flat-top distribution. Similar effect is observed as the repetition period of chorus elements becomes shorter, with the additional effect of increased electron precipitation due to transition from bursty to continuous flux profiles in the loss cone. These findings highlight the importance of incorporating nonlinear effects and fine-scale wave properties in the future development of high-energy electron models for the outer radiation belt.

Key Points:

- A new numerical wave model and particle simulation method is used to study nonlinear resonant interaction of electrons with chorus waves
- Adding fine structure to chorus waves changes the pitch angle distribution of accelerated electron from butterfly to flat-top shape
- Shorter repetition periods lead to faster bounce-phase-mixing and increase the average flux in the loss cone

Supporting Information:

Supporting Information may be found in the online version of this article.

Correspondence to:

M. Hanzelka,
mirekhanzelka@gmail.com

Citation:

Hanzelka, M., Shprits, Y., Wang, D., Haas, B., Santolík, O., & Gan, L. (2025). Effects of fine spectral structure of chorus emissions on nonlinear scattering and acceleration of radiation belt electrons. *Journal of Geophysical Research: Space Physics*, *130*, e2024JA033382. https://doi.org/10.1029/2024JA033382

Received 28 SEP 2024
Accepted 10 MAR 2025

Author Contributions:

Conceptualization: Miroslav Hanzelka, Yuri Shprits, Ondřej Santolík, Longzhi Gan
Data curation: Miroslav Hanzelka
Formal analysis: Miroslav Hanzelka, Bernhard Haas
Funding acquisition: Miroslav Hanzelka, Yuri Shprits
Investigation: Miroslav Hanzelka
Methodology: Miroslav Hanzelka
Project administration: Miroslav Hanzelka, Yuri Shprits
Resources: Yuri Shprits
Software: Miroslav Hanzelka, Bernhard Haas
Supervision: Yuri Shprits

1. Introduction

Particle scattering by plasma waves plays a crucial role in the dynamics of relativistic electrons in Earth's outer radiation belt (Baker, 2021; Friedel et al., 2002; Li & Hudson, 2019; Shprits, Elkington, et al., 2008, Shprits, Subbotin, et al., 2008; Thorne, 2010). The radiation hazard posed by these high-energy electrons to spacecraft instruments has made them a topic of extensive research. Given the limited spatial coverage of in-situ probes, physics-based numerical models are essential for understanding the global evolution of radiation belt electron populations (Beutier & Boscher, 1995; Glauert et al., 2014; Subbotin & Shprits, 2009; Varotsou et al., 2005). The standard approach to modeling wave-particle scattering involves solving the Fokker-Planck equation using diffusion coefficients from the quasilinear approximation of the Vlasov equation (Glauert & Horne, 2005; Kennel & Engelmann, 1966; Lyons, 1974), which assumes small particle trajectory perturbations due to incoherent waves (Allanson et al., 2022; Lemons et al., 2009; Volokitin & Krafft, 2012). Numerical simulations of this type have successfully reproduced enhancements and losses of relativistic electron populations observed during geomagnetic storms (Li, Ma, et al., 2016; Reeves et al., 2012; Subbotin et al., 2011).

However, large-amplitude, coherent waves such as whistler-mode chorus violate the assumptions of diffusive models. Chorus waves, with magnetic field amplitudes reaching up to 1% of the ambient field (Li et al., 2011; Santolík, Gurnett, et al., 2003; Tsurutani & Smith, 1974), induce significant electron pitch angle and energy changes during single interactions (Bortnik et al., 2008; Omura & Summers, 2006). These interactions create nongyrotropic electron distributions and require a fully nonlinear treatment, particularly for large perturbation effects like phase trapping and anomalous scattering (Albert et al., 2022). Nonlinear interactions between electrons and other waves, such as Electromagnetic Ion Cyclotron (EMIC) waves, have also been observed and

Validation: Miroslav Hanzelka, Dedong Wang
Visualization: Miroslav Hanzelka
Writing – original draft: Miroslav Hanzelka
Writing – review & editing: Miroslav Hanzelka, Yuri Shprits, Dedong Wang, Bernhard Haas, Ondřej Santolík, Longzhi Gan

simulated (Grach & Demekhov, 2020; Omura et al., 2013). In addition, oblique wave propagation can extend the energy range of resonant interaction through harmonic cyclotron and Landau resonances (G. Wang et al., 2017; Omura et al., 2019; Hanzelka et al., 2023), which can also drive nonlinear scattering.

While quasilinear theory fails for large-amplitude waves over short timescales (Allanson et al., 2021; L. Chen et al., 2021; Gan et al., 2023), the applicability of the diffusive paradigm on longer timescales of minutes to hours remains a topic of debate (Ripoll et al., 2020; Tu et al., 2019). Some studies have presented rescaled diffusion coefficients for nonlinear regimes (Artemyev et al., 2022), achieving better agreement with measured storm-time electron fluxes (Kondrashov et al., 2024). Others have highlighted the inherent nondiffusive nature of resonant electron dynamics using methods based on test-particle simulations (Tao et al., 2014) and chaotic maps of the jump processes (Artemyev et al., 2020; Lukin et al., 2024). Zheng et al. (2019) argued that diffusion and advection coefficients become meaningless in regimes with large stochastic changes, advocating for the use of Markov matrices (a form of numerical Green's function (GF) of electron response) obtained from test-particle simulations to evolve the electron distribution. These approaches have demonstrated increased electron acceleration from nonlinear interactions with chorus waves (Furuya et al., 2008; Hsieh et al., 2020, 2022; Kubota & Omura, 2018; Omura, Miyashita, et al., 2015).

Incorporating nonlinear effects into radiation belt models also requires accurate wave field parametrization. Unlike quasilinear models, where averaged wave power is used (Meredith et al., 2012; Orlova & Shprits, 2014; Li, Santolik, et al., 2016; Agapitov et al., 2018; D. Wang et al., 2019; Wong et al., 2024; Santolík et al., 2024), nonlinear interactions depend on fine spectral features, such as chirp rate and subpacket amplitude modulations (Foster et al., 2021; Santolík, Gurnett, et al., 2003, Santolík, Kletzing, et al., 2014). Incoherence in chorus rising-tone packets represents another important feature as it can reduce electron acceleration efficiency, but rapid successive trapping can still drive significant acceleration even for these quasi-coherent waves with broader frequency bands (Artemyev et al., 2022; Hiraga & Omura, 2020; Zhang et al., 2020). Therefore, millisecond variations in amplitude and phase must be accurately characterized in numerical models of nonlinear wave-particle interactions.

This study aims to answer the following question: What role do fine-spectral structures of chorus waves play in the formation of radiation belt electron populations? We address it by exploring frequency bandwidth, wave normal angle (WNA) distribution, and repetition period of chorus elements' impact on the electron acceleration to ultrarelativistic energies. Using a new simulation method based on Liouville mapping of phase space density (PSD) (Section 2), we observe rapid acceleration to >1 MeV energies and show that fine spectral features of chorus emissions suppress the previously predicted (Hsieh et al., 2020; Saito & Miyoshi, 2022) formation of peaks in the electron pitch-angle distribution (PADs) (Section 3). Our findings thus suggest that to fully understand the behavior of relativistic electron populations during geomagnetically active periods, radiation belt models must account for the fine structure of wave fields and nonlinear scattering processes.

2. Methods

2.1. Wave Model

The wave model employed in this study was designed to capture fine spectral features of quasiparallel rising-tone chorus elements, while retaining a simple structure that allows for parametric analysis of the respective features. The wave element is constructed through the summation of chirping wave packets with random initial phases, which agrees with the spacecraft observations presented by Santolík, Kletzing, et al. (2014) and Crabtree et al. (2017), where the detected phase variations hint at a narrow incoherent spectrum. Due to computational constraints, we assume that the wave energy propagates exactly along a dipole magnetic field line (ducted propagation, justified by the investigations of Hanzelka and Santolík (2019), L. Chen et al. (2022), Kang et al. (2024), and others), thus reducing the spatial dimensions to the field-aligned distance h.

The construction of the spatio-temporal structure of a model chorus element can be summarized in the three following steps:

1. The wave energy density and frequency of each elementary chirping wave are evolved in time (t) and space (h) through transport equations solved numerically by an upwind scheme. Compared to the previous work of (Hanzelka et al., 2020), the nonlinear growth term, important near the equatorial source region, is removed and replaced instead by a simple ramp-up function in amplitude/energy.

2. The wave energy density is converted to magnetic field amplitude using the cold plasma dispersion relation (Stix, 1992), and the waves from the first step are summed. Each wave represents a single chirping frequency (ω) and WNA (θ) component of the spectrum, and is weighted so that the resulting rising-tone element has a Gaussian amplitude distribution in frequency (mean $\omega_0(t)$, standard deviation σ_ω) and a half-Gaussian distribution in wave normal angles (mean 0°, standard deviation σ_θ), taking into account the $\sin\theta$ term in the Jacobian of transformation from the spherical coordinates (Santolík, Kletzing, et al., 2014). The peak amplitude in time and space is fixated after this step.
3. The final summed field is then decomposed into instantaneous phases and amplitudes using the Hilbert transform. These quantities are transferred to a coarse grid and saved for use in the test-particle simulation.

This form is suitable for quasicoherent chorus elements with narrow bandwidth since larger ones increase the number of phase jumps and thus require finer grids. At each particle's position, bilinear interpolation in space and time is performed to obtain the electric ($\mathbf{E_w}$) and magnetic ($\mathbf{B_w}$) whistler-mode wave fields. To reduce the number of quantities to be interpolated, the phase ψ of each electric and magnetic field is the same in each component, namely, it is the phase obtained from Hilbert transform of the B_{wx} component (with the ±90° and ±180° phase shifts between components included). The ellipticity of polarization (Santolík, Parrot, & Lefeuvre, 2003) is set to 1 since quasiparallel chorus waves poses a nearly circularly polarized magnetic field (Remya et al., 2016).

With this model, we analyze the effects of WNA distribution and bandwidth of lower-band rising-tone chorus elements on the radiation belt electrons. We prepare wave fields of nine chorus elements, combining three bandwidth values $2\sigma_\omega = \{0.0, 0.01, 0.025\}\Omega_{e0}$ (48 chirping wave samples) and three wave normal distribution widths $2\sigma_\theta = \{0°, 20°, 45°\}$ (24 chirping wave samples). Here, Ω_{e0} stands for the equatorial electron gyrofrequency in the heart of the radiation belt at $L = 5.5$, corresponding to an ambient field strength $B_{0eq} = 186.3$ nT. The electron plasma-to-gyrofrequency ratio ω_{pe0}/Ω_{e0} is set to 5.0 at the equator, and the plasma frequency increases as $1/\cos\lambda$, where λ is the magnetic dipole latitude (this corresponds to a dipole approximation of the Denton et al. (2002) field line density model with a power law coefficient $\alpha = 0.5$). The peak amplitude of the element with $2\sigma_\omega = 0.01\Omega_{e0}$ and $2\sigma_\theta = 20°$ is set to $0.01B_{0eq}$, and the other elements are renormalized so that B_w^2 averaged over time and space is constant in all simulations. Repetition period of chorus elements is taken into account, with the implementation explained in Section 2.2. Each of these wave fields is symmetric around the equator, thus preserving the North-South symmetry of the studied system. For a complete set of input values, boundary conditions, smoothening functions, and other details pertaining to the numerical model, see Text S1 and Table S1 in Supporting Information S1.

In Figure 1, we plot selected properties of the chorus element with bandwidth $2\sigma_\omega = 0.01\Omega_{e0}$ and WNA distribution width $2\sigma_\theta = 20°$. We can see that the model exhibits subpacket structure and frequency jumps similar to observations from Van Allen Probes and Cluster spacecraft (Foster et al., 2021; Santolík et al., 2004, Santolík, Kletzing, et al., 2014), while being less regular than the models based on nonlinear chorus growth equations (Hanzelka et al., 2021; Hsieh et al., 2020; Kubota et al., 2018). Note that in Figure 1, information about amplitude envelopes and frequencies of all components was used, while the input for the test-particle simulation uses the simplified form as described above.

2.2. Test-Particle Simulations

We present a novel numerical method for tracking the evolution of electron PSD that remains stable without the use of additional stabilization operators (Zheng et al., 2019) or very fine coordinate grids (Omura, Nakamura, et al., 2015), which are required in the GF method. Similar to the GF approach, our method is based on test-particle tracing. The trajectories of electrons moving through the wave fields described in Section 2.1 are calculated as solutions to the equations of motion prescribed by the Lorentz force. The effects of the mirror force in the ambient dipole field are calculated by first-order Taylor expansion, and the field line curvature effects are excluded (Bell, 1984). The trajectory integration is performed with the phase-corrected relativistic Boris method (Zenitani & Umeda, 2018). Our implementation uses adaptive time steps, which allows us to use larger time steps in the weak field region near the equator. Numerical test with our model have shown that 24 steps per local gyroperiod is enough to resolve the nonlinear effects on particle trajectories near the resonance. In regions where the wave field drops to zero, the time step is increased to 4 points per local gyroperiod.

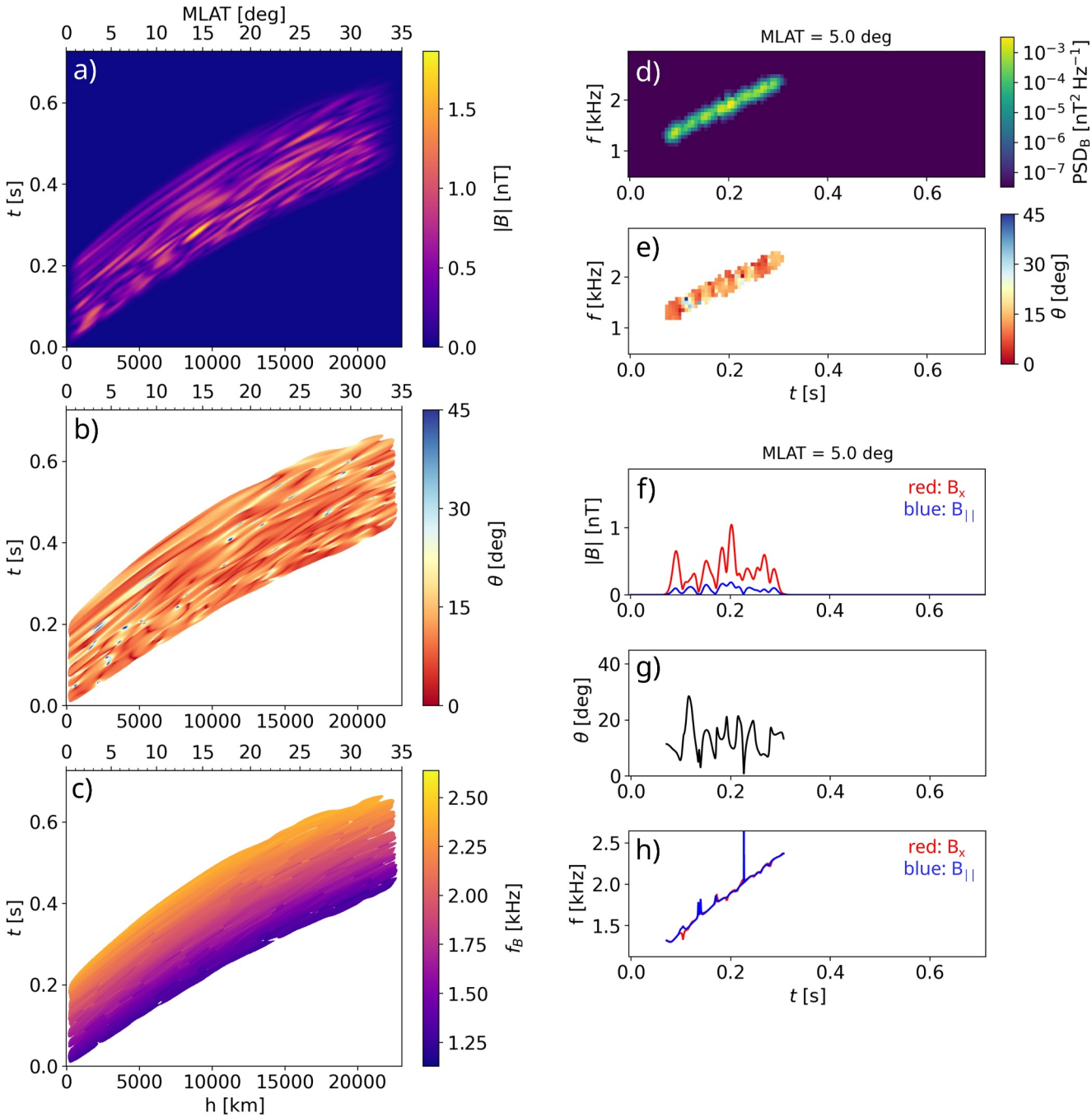

Figure 1. Example of a rising-tone chorus element produced by the simulation procedure described in Section 2.1. The frequency and wave normal angle (WNA) distributions are defined by widths of (half-)Gaussian distributions $2\sigma_\omega = 0.01\Omega_{e0}$ and $2\sigma_\theta = 20°$. In the left column (panels a–c), space-time plots of amplitude, WNA, and instantaneous frequency (power-averaged over all magnetic field components) are presented. Field-aligned distance is converted to magnetic latitude. Panels (d) and (e) show the power spectral density and WNA as time-frequency spectrograms constructed from a time series recorded at MLAT = 5°. The last three plots, (f)–(h), show line plots of the amplitude envelope (B_x and $B_{||}$), WNA, and the instantaneous frequency (of B_x and $B_{||}$). Data below the threshold of $10^{-4}\max(B_w^2)$ were removed in panels (b)–(c), (e), and (g)–(h).

Additionally, gyromotion outside of the wave simulation box is not resolved. Instead, we use a lookup table for the time spent during adiabatic motion between two latitudes (see Text S2 in Supporting Information S1 for more details). Particles that reach the atmosphere are considered lost and are ignored for the rest of the simulation run. Particles that return to the boundary of the wave simulation box have their energy and equatorial pitch angle

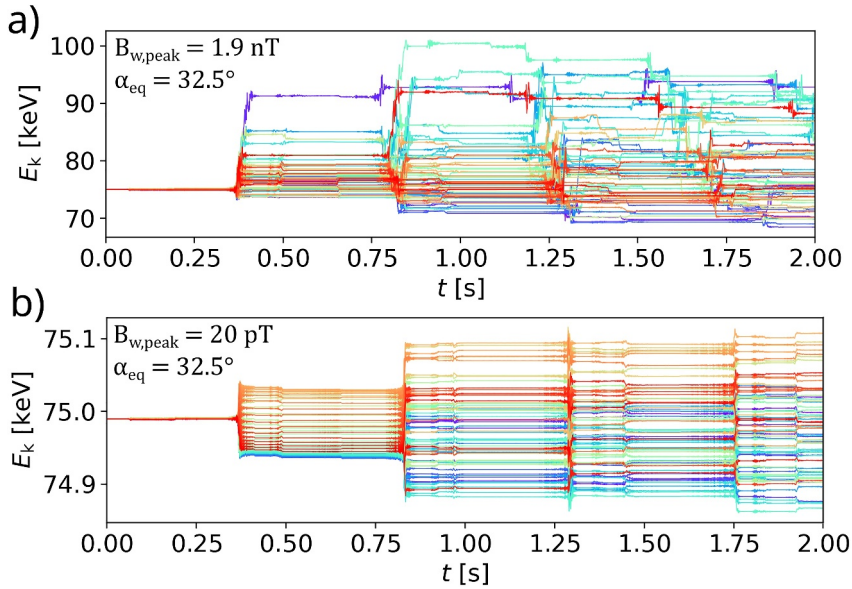

Figure 2. Illustration of energy changes experienced by electrons interacting with quasiparallel, quasicoherent chorus wave with repeating elements. The 64 electrons in this test run were traced for 2 s and started from the equator with equatorial pitch angle $\alpha_{eq} = 32.5°$ and energy $E_k = 75$ keV. The initial gyrophase is sampled uniformly and represented by different line colors. (a) Interaction with high amplitude elements peaking at 1.9 nT (maximum across the entire simulation box). (b) Similar to panel (a), but with the peak amplitude decreased to 20 pT.

preserved, and their gyrophase is randomized. This randomization is commonly used in particle-in-cell simulations (Hikishima & Omura, 2012; Nogi et al., 2020) and it is well-justified because nongyrotropic structures formed through nonlinear interactions experience fast velocity dispersion (Trakhtengerts et al., 2003). In cases where the particle ends up outside of the wave field when the time limit is reached, the look-up table is inverted to obtain the final latitude (field-aligned distance).

Energy evolution along example trajectories of electrons interacting with high-amplitude chorus elements is presented in Figure 2a to demonstrate the typical nonlinear behavior. The peak amplitude is set to 1.9 nT, and the frequency and WNA distribution parameters are $2\sigma_\omega = 0.025\Omega_{e0}$ and $2\sigma_\omega = 45°$. During the 2 s of the simulation run, the electrons with initial energy of 75 keV and equatorial pitch angle 32.5° experience 4 or more phase trapping or phase bunching interactions. Despite the low gyrophase sampling (64 points per full angle) and the short subpacket modulations (less than 10 ms on average), significant acceleration through phase trapping is observed in several particles. Noticeably, the distribution of electrons in energy is strongly nonuniform after the first interaction, but becomes progressively more uniform over time. In contrast, the energy evolution of particles interacting with a weaker wave in Figure 2b does not show any signatures of phase trapping, and the spread in energies is quite uniform already after the first interaction. The wave field used in this second example has the same spatio-temporal structure, but the peak amplitude has been rescaled to 20 pT.

To study the changes in electron PSD, the time direction is reverted in our simulation, tracing particles from a future point t_1 backward to time t_0 where the PSD distribution $f(t_0)$ was known. Liouville's theorem for Hamiltonian systems asserts that the PSD remains constant along the particle trajectories, allowing us to equate $f(h(t_0), E_k(t_0), \alpha_{eq}(t_0), \varphi(t_0))$ with $f(h(t_1), E_k(t_1), \alpha_{eq}(t_1), \varphi(t_1))$ (Hanzelka et al., 2021; Nunn & Omura, 2015). Here, E_k stands for energy, α_{eq} for the equatorial pitch angle, and φ is the gyrophase angle. We use an initial distribution that is bi-Maxwellian in momenta (Summers et al., 2012) to represent the seed electron population before increase in wave activity, with initial PSD in the loss cone set to zero (see Text S2 and Figure S1 in Supporting Information S1).

When the distribution at t_1 is obtained, we can utilize the already known initial and final points of particle trajectories to repeat the mapping over an arbitrary number of cycles. This way, we can obtain the state of the PSD distribution after several interactions with the same element. In our current implementation of this numerical mapping technique, the traced particles start on a uniform grid in h, $\log_{10} E_k$, α_{eq}, and φ. Thus, when mapping

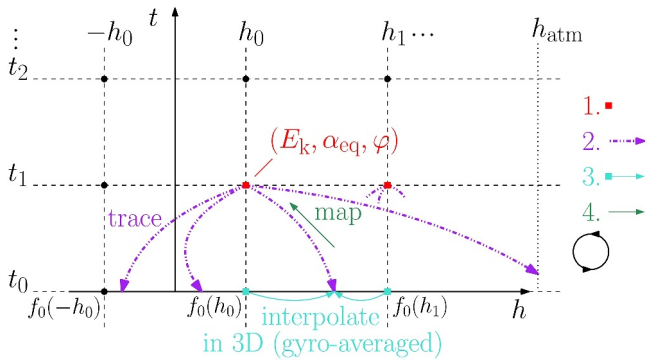

Figure 3. Schematic explanation of the mapping procedure. Starting at t_1, particles are traced back from grid points along the northern half of a selected field line (red squares). In each of these points, the velocity space is sampled using the 3D grid of energies, equatorial pitch angles, and gyrophases. Particles are traced back in time (purple dash dot dotted arrows) to t_0 where the initial gyrotropic phase space density (PSD) distribution in (h, E_k, α_{eq}) was known. PSD at the particle position at t_0 is obtained through multilinear interpolation (turquoise squares and arrows). Note that in the first step, the analytic formula for the initial distribution can be used. Finally, PSD is mapped along trajectories to the future time point t_1 (green arrow) and then gyroaveraged. The process then repeats with the precalculated trajectories shifted to t_2, t_3, …, representing interaction with a periodic wave field.

from t_i to t_{i+1}, $i \neq 0$, we need to interpolate $f(t_i)$ to trajectory endpoints. A schematic explanation of the mapping procedure is presented in Figure 3. After a desired number of mapping cycles, we obtain a perturbed electron PSD distribution in the (h, E_k, φ) space. To produce results comparable with quasilinear simulation results from recent literature, we require a bounce-averaged distribution. The averaging is done by summing along the h-coordinate with weights given as the particle dwell time in each bin during adiabatic motion. The dwell times are obtained from the lookup table used above to trace particles outside of the wave field.

In all simulation runs, the initial grid is set as linear in h, α_{eq}, and φ, and logarithmic in E_k. The grid points lie in centers of the bins, with the outermost bin edges defined by the coordinate ranges in the table. The total number of grid points is 132 710 400, of which 53 982 720 have (h, α_{eq}) value pairs permitted in the dipole field configuration. The total simulation time $t_{tot} = 0.8$ s is an integer multiple of the three selected wave repetition periods 0.2 s, 0.4 s, and 0.8 s, which is needed for smooth connection in the periodic mapping procedure. The periodically repeating wave field is implemented by summing the contributions evaluated at times $t \pm \ell T_{rep}$, where ℓ is an integer running from $-t_{tot}/T_{rep} + 1$ to $+t_{tot}/T_{rep} - 1$. At the end of the simulation period, wave fields along the whole field line are slowly driven to zero to prevent nonresonant scattering on sharp packet boundaries (L. Chen et al., 2016)—the same treatment is applied at the start of the simulations. For further technical details related to the particle tracing and mapping methods, see Text S2 and Table S2 in Supporting Information S1.

3. Results

3.1. Effects of Frequency Bandwidth and WNA Distribution

We ran the mapping procedure for $N = 512$ cycles (approximately 410 s, or 7 min) to simulate electron interaction with a long train of chorus elements. The nine wave field models with various bandwidths and wave normal distributions from Section 2.1 were used to assess the importance of chorus fine structure in electron acceleration and pitch-angle scattering, with the repetition period fixed to $T_{rep} = 0.4$ s. First, we examined the time evolution of the energy profile by studying the quarter-bounce-averaged distributions integrated over all pitch angles. As demonstrated in Figure 4 for a parallel propagating element without subpacket modulation, the initial Maxwellian profile started converging toward a power-law profile at lower energies up to about 300 keV. Within less than a minute (turquoise line), PSD at energies above 1 MeV reached the chosen threshold of $10^{-10}\max(f_0)$, while initially, only electrons with $E_k < 600$ keV had PSD above this threshold. After 7 min (red line), energies of 6 MeV are reached. Results obtained for a quasiparallel chorus element with fine structure ($2\sigma_\omega = 0.025\Omega_{e0}$ and $2\sigma_\theta = 45°$) were not significantly different, thus establishing that the microscopic variations in the wave field have little impact on the overall energization of the seed electron population. Our conclusion differs from the results of Kubota and Omura (2018) who observed increased acceleration rates up to 4 MeV when wave amplitude modulations were included in their simulations. This highlights the importance of including not only amplitude modulations but also phase jumps in chorus wave models, as these reduce the efficiency of nonlinear acceleration (Zhang et al., 2020).

The impact of wave parametrization becomes more apparent when examining PADs. Figure 5 shows the averaged electron PSD distribution after $N = 512$ mapping cycles, with each panel corresponding to one of the nine wave parametrizations. The train of parallel chorus elements with no subpackets (Figure 5a) results in the formation of a peak in the PAD at around 1 MeV and above. At these energies, ultrarelativistic resonant acceleration happens when the electron propagates in the same direction as the whistler wave (Hiraga & Omura, 2020). The peak shifts to lower pitch angles as the energy increases. A similar feature has been observed by Hsieh et al. (2020) using the numerical GF method. With increasing frequency bandwidth (or correspondingly, shorter subpackets), acceleration near $\alpha_{eq} = 90°$ is slightly enhanced, and the peak at high energies becomes less prominent (Figures 5a–5c).

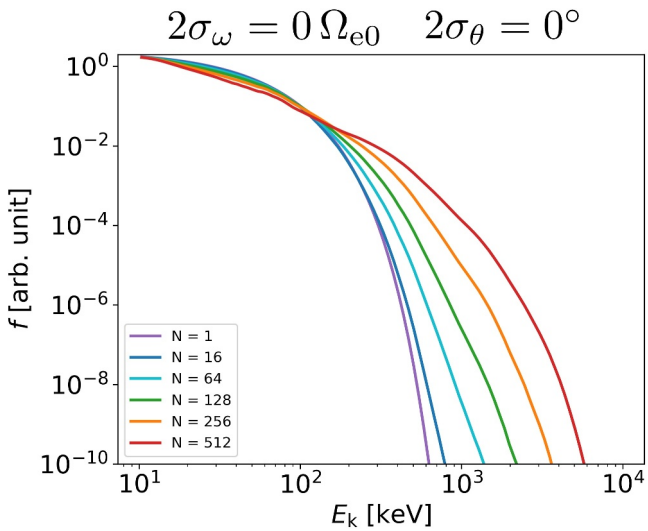

Figure 4. Evolution of the electron energy spectrum during interaction with a parallel propagating chorus element without fine structure. The line colors represent the number of cycles in the mapping procedure, $N = \{1, 16, 64, 128, 256, 512\}$, which translates to {0.8, 12.8, 51.2, 102.4, 204.8, 409.6} seconds. Simulation results from runs with fine structure included into the wave models present negligible changes and are therefore not plotted here.

The impact of broadening WNA distribution is shown in Figures 5a, 5d, and 5g. As the wave becomes more oblique, the PAD peak at higher energies disappears and is replaced by a flat-top distribution. The acceleration near 90° is significantly enhanced, but as discussed in the presentation of Figure 4, the electron density at ultrarelativistic energies is not impacted. The main effect of varying the wave normal angles is thus the redistribution of electrons in pitch angle. Increasing the frequency bandwidth of quasiparallel waves (Figures 5g–5i) leads to a minor decrease in PSD at high energies, while the PAD profiles remain mostly unchanged.

3.2. Effects of Chorus Repetition Period

All results in Section 3.1 were obtained using a chorus repetition period of $T_{rep} = 0.4$ s. In Figure 6, we present simulation results for parallel chorus elements without subpackets with repetition periods of 0.2 s, 0.4 s, and 0.8 s. Panels a–c show how quickly the local PSD distributions converge to the quarter-bounce-averaged distribution. After $N = 8$ mapping steps, the local distributions in the case with the shortest period are already bounce-phase mixed, whereas $N = 16$ or more steps are needed in the cases with longer repetition periods to reached a bounce-phase-mixed state where the distribution is independent of latitude. Within about 10 degrees of the (anti-)loss cone, the PADs never fully relax due to ongoing atmospheric losses and strong anomalous scattering.

Figures 6d–6i show the effect of repetition period on the final state of the simulated PSD at $N = 512$ (~7 min). The high-energy peak in the PADs, characteristic of interaction with parallel waves without amplitude modulations, is most prominent when $T_{rep} = 0.8$ s, and becomes more spread out as the period shortens. Furthermore, the position of the peak shifts to higher pitch angles with decreasing T_{rep}: at the 5.4 MeV energy level, the peak occurs approximately at $\alpha_{eq} = 45°$ for $T_{rep} = 0.8$ s, and at $\alpha_{eq} = 55°$ for $T_{rep} = 0.2$ s. We speculate that this arises from the overlap of resonance islands of adjacent chorus elements at ultrarelativistic energies, which may reduce the acceleration efficiency.

Another significant difference is observed at energies below 100 keV, where losses are weaker in the $T_{rep} = 0.8$ s case (see PSD values at $\alpha_{eq} < 3°$ in Figure 6d, compare with Figures 6e and 6f). Correspondingly, the loss cone filling is lower at those energies, indicating the bursty nature of the precipitation. Even when the wave has a large enough time-averaged amplitude to completely fill the loss cone after a resonant interaction, the localization of this power into packets (elements) can decrease the total precipitation. Aside from these impacts on particle loss, we may conclude that the rate at which electrons are accelerated to relativistic energies does not exhibit any apparent dependence on T_{rep}.

4. Summary and Discussion

In this study, we introduced a new numerical PSD mapping method for simulating nonlinear interaction of particles with electromagnetic waves. We used this method to analyze the effects of spectral structure and fine modulations of lower-band chorus elements on the acceleration of electrons and the pitch angle profiles of the perturbed PSD. The main findings can be summarized as follows:

1. A seed population of electrons (10 keV to 300 keV), when accelerated by a train of chorus elements with a parallel propagation direction and no amplitude modulations, can reach ultrarelativistic (>2 MeV) energies within a few minutes. The high-energy population forms a butterfly distribution in pitch angle, with the peak moving from 75° (1 MeV) to 45° (5 MeV).
2. Increasing width of the WNA distribution enhances acceleration near $\alpha_{eq} = 90°$, making the butterfly-shaped PAD transition to a flat-top distribution. Similar effect is induced by an increase in frequency bandwidth and by a shorter repetition period of individual elements.

Apart from these main highlights, we reported other two noteworthy results:

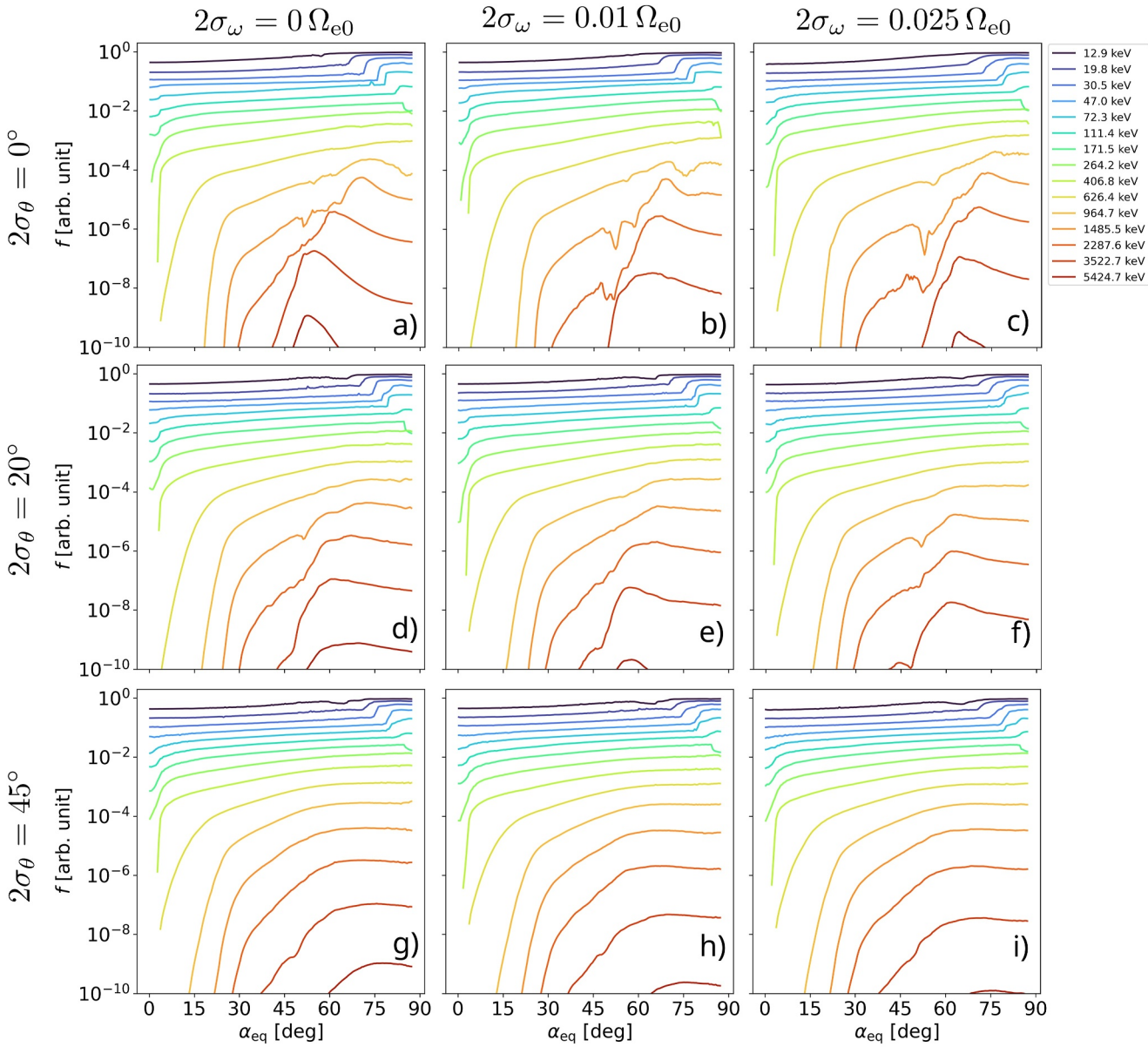

Figure 5. Pitch-angle distributions across various energy levels after $N = 512$ mapping cycles. Each row corresponds to a different WNA distribution ($2\sigma_\theta = 0°$ in panels a–c, $2\sigma_\theta = 20°$ in panels d–f, $2\sigma_\theta = 45°$ in panels g–i) and each column corresponds to a different frequency bandwidth ($2\sigma_\omega = 0\Omega_{e0}$ in the first column, $2\sigma_\omega = 0.01\Omega_{e0}$ in the second column, and $2\sigma_\omega = 0.025\Omega_{e0}$ in the third column).

3. In the seed electron energy range, the PAD reaches a bounce-phase-mixed state within less than 10 s for short repetition periods of chorus elements ($T_{rep} = 0.2, s$) and within less than 30 s for longer periods ($T_{rep} = 0.8, s$). An exception is observed at pitch angles near the loss cone and the anti-loss cone, where a bounce-phase-mixed state is never reached.
4. When T_{rep} is significantly larger than the duration of the element, precipitation will occur in bursts, and the loss cone will be only partially filled on average. Consequently, the loss rate associated with scattering by waves with sufficiently high average wave power to drive strong diffusion may be less than predicted by wave models that omit the discrete nature of chorus emissions.

To carefully interpret and discuss our results, we must start by considering the limitations of our simulation methods. The accuracy of predictions regarding PSD evolution driven by wave-particle interactions is highly dependent on the quality of the wave model. Test-particle methods require detailed waveform information along

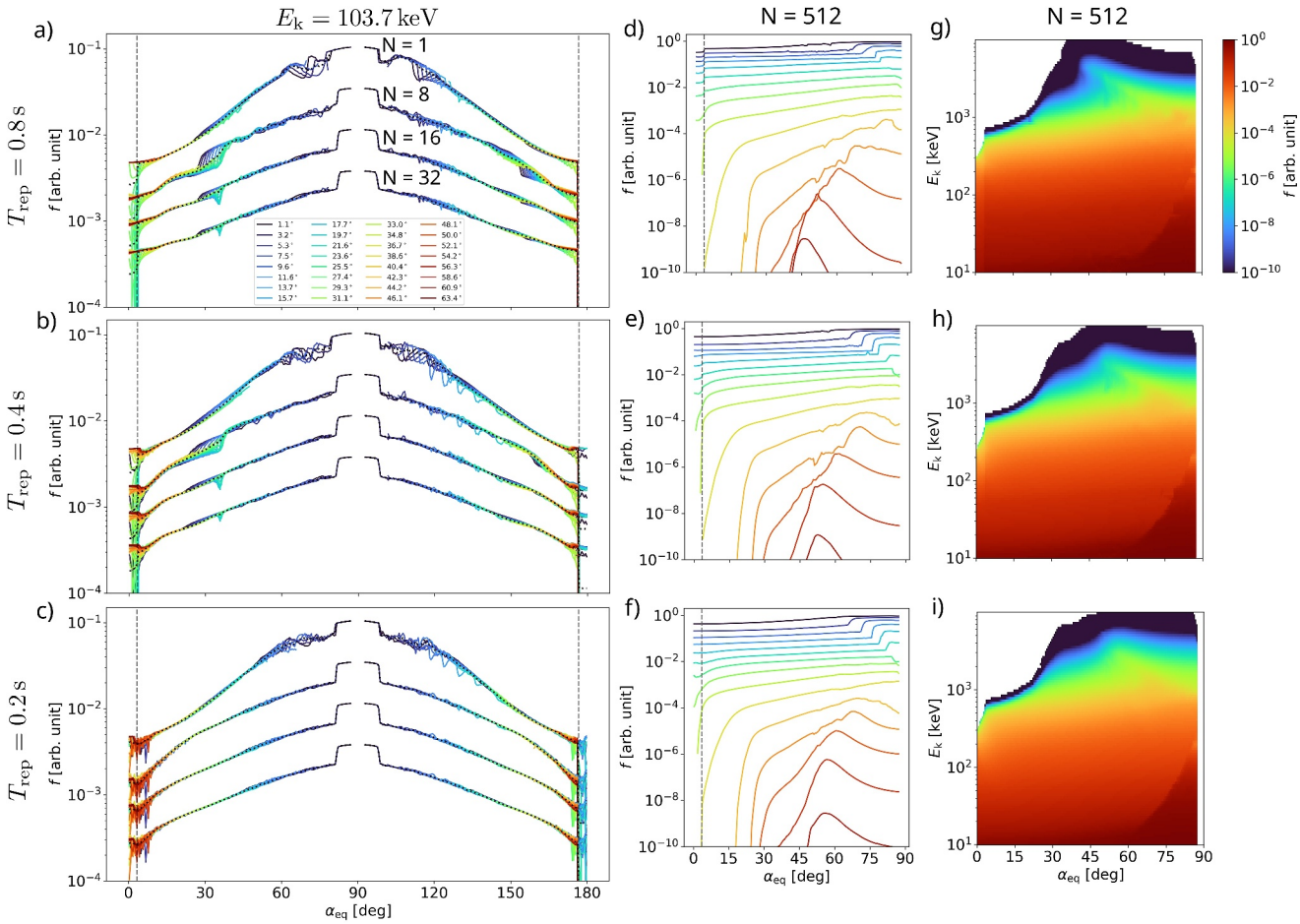

Figure 6. The effects of chorus repetition period T_{rep} on the phase space density (PSD) evolution, with each row corresponding to one of the three values 0.8 s, 0.4 s, and 0.2 s. In all three cases, the wave field is parametrized by $2\sigma_\omega = 0\ \Omega_{e0}$, $2\sigma_\theta = 0°$. The first column (panels a–c) shows the state of local PADs at four different time points given by the number of cycles $N = \{1, 8, 16, 32\}$; the energy value is always the same, $E_k = 104.7$ keV. As the number of cycles increases, the PSD values are multiplied by $1/3$ each time to fit all lines into one plot without major overlaps. The second column (panels (d)–(f)) shows the PADs at $N = 512$ across several energy levels coded by color, with the same legend as in Figure 5. The dashed gray lines in panels a–f represent the equatorial loss cone. The third column (panels (g)–(i)) shows the two-dimensional PSD distribution in energies and equatorial pitch angles as a heatmap.

the field line, which must be simulated to match local observations. Unfortunately, there is currently no comprehensive study showing the dependence of chorus fine structure on latitude. Models like those used by Kubota and Omura (2018), Hsieh et al. (2020), or Hanzelka et al. (2021), based on a highly coherent growth process described by the nonlinear chorus equations (Omura et al., 2009), exhibit a very regular subpacket structure that remains near constant along the field line. In contrast, spacecraft observations reveal a less coherent structure of chorus elements with frequent phase jumps and variable depths of modulation (Santolík, Kletzing, et al., 2014; Zhang et al., 2021). This quasicoherent nature of chorus is well captured by our model. However, self-consistent simulations of wave generation reveal that in the near-equatorial region, the presence of the nonlinear resonant current makes the wave structure more coherent (H. Chen et al., 2024). This is especially true for the low-frequency tail of the chorus element, which was experimentally confirmed to exhibit weaker and longer amplitude modulations (Crabtree et al., 2017). Furthermore, the source of chorus elements is known to drift upstream, creating a region where the northward and southward propagating packets overlap. Our wave model can incorporate a shifted source, and the increased coherence of the low frequency tail can be achieved by introducing a time dependent bandwidth $\sigma_\omega(t)$. These features have been omitted in this study since the latitudinal extent of the waves is large and thus the near-equatorial behavior should not have a significant impact on the interaction with electrons. Further, we have not included the growth in wave energy density due to field line convergence (Hanzelka & Santolík, 2019). While there is a statistical trend showing the growth of average whistler-mode wave

amplitudes with latitude up to about MLAT $= 40°$ (Santolík, Macúšová, et al., 2014), it is unknown whether this trend reflects the behavior of high-amplitude rising-tone elements.

Unlike Hsieh et al. (2020, 2022), we have not studied any highly oblique waves in our simulation, focusing instead on the quasiparallel case. There are two reasons for this choice. Firstly, quasiparallel lower band chorus is dominant in the outer radiation belt and has much higher average power than oblique chorus (Taubenschuss et al., 2014). Secondly, oblique waves cannot be efficiently guided by density structures and may experience strong damping as they propagate to higher latitudes (Hanzelka & Santolík, 2019), which would require a more advanced wave model. More importantly, since unducted whistler-mode waves propagate across L-shells, our field-aligned simulations would not strictly suffice. Falling-tone elements have not been considered due to their low occurrence rates (Li et al., 2011).

Another major challenge in chorus wave modeling is the discrete, periodic nature of the wave field. Since particle tracing is performed for only one cycle within our simulation, a selected particle will always enter the wave field with the same difference between the wave phase and gyrophase and always experience the same type of interaction (e.g., phase trapping). In a more realistic scenario, the rising tone elements in a chorus burst are not identical, and even a slight change can result in a very different trajectory of individual particles. As a result of this simplified model with exact periodicity, certain irregular features persist in the PSD mapping procedure (see the $E_k = 1485$ keV line in Figures 5a–5c). Zheng et al. (2019) resolved this problem within the framework of the numerical GF method by performing an ensemble average over simulations with different initial phases. A similar approach could be employed in our method by randomly alternating between maps obtained for wave fields with varying initial phases. However, particle tracing is the most computationally expensive step of our method, and so to perform this ensemble averaging for each set of wave model parameters, we need to explore ways of reducing the number of particles required to achieve the desired accuracy in PSD values. This might be achieved by replacing the uniform sampling of the $(h, E_k, \alpha_{eq}, \varphi)$ space with quasirandom sampling base on low-discrepancy sequences, similar to the methods used in Monte Carlo simulations. Another modeling challenge relates to ensemble averaging over the chorus repetition phase—a shift in this phase would result in a mismatch in wave fields between neighboring maps. This is a general issue with short repetition periods, where the transition from one model element to another requires a special map. In fact, the $T_{rep} = 0.4$ s and $T_{rep} = 0.2$ s simulations in Section 3 should have a special start map and end map, but this was omitted due to the decreasing impact of these maps with increasing number of cycles N. As shown in the Time History of Events and Macroscale Interactions during Substorms (THEMIS) spacecraft data presented by Shue et al. (2015), the repetition period of lower-band chorus has a large spread, with very short periods of 0.1s being about as common as longer periods of 1 s. Therefore, chorus trains with short repetition periods form a large portion of the events and must be considered in numerical models like ours.

With the limitations of the applied method properly considered, we move to the interpretation of our results. In the description of Figure 4, we noted that the energy spectrum is not strongly affected by changes in the frequency bandwidth (σ_ω) and WNA distribution (width σ_θ). This suggests that the fine structure of chorus elements is not crucial for estimation of the energy profile. The incorporation of chorus fine structure into the wave model becomes important in the formation of the pitch angle profile of high-energy electrons. What is significant here is the quick disappearance of the peak near $\alpha_{eq} = 60°$ with increasing values of σ_ω and σ_θ (Figure 5), suggesting that the formation of butterfly distributions proposed by Saito and Miyoshi (2022) is unlikely. According to THEMIS spacecraft measurements analyzed by Gao et al. (2014), the typical frequency bandwidth of rising tone chorus elements at $L = 5.5$ is about $2\sigma_\omega = 0.015\Omega_{e0}$, and Santolík, Kletzing, et al. (2014) estimate the median of WNA values from a Van Allen Probes dataset of high-amplitude risers to be approximately 15° (corresponding to a standard deviation $\sigma_\theta = 22°$ for a half-normal distribution). Figure 5h, which is closest to these typical values, shows that we should expect to see a flat-top distribution in the accelerated electron population.

The effect of discrete spectral structure of chorus on electron scattering, discussed in Section 3.2, has been previously studied by Tao et al. (2014). They have demonstrated with test-particle simulations that when the trapping period is large, the quasilinear theory deviates from the nonlinear results. While we do not compare our results with the quasilinear approach in this study, some of our findings are relevant to the applicability of numerical modeling based on Fokker-Planck equations with bounce-averaged diffusion coefficients. Results presented in Figures 6a–6c reveal that even when the trapping period is much larger than the duration of the chorus element, a bounce-phase-mixed state is reached on the scale of tens of seconds, demonstrating that models

utilizing bounce-averaged PSD distribution could be appropriate even for high-amplitude discrete emissions. The electron behavior near the loss cone presents an exception (see Figures 6a–6c), as the loss process driven by coherent or quasicoherent waves prevents the distribution from reaching the bounce-phase-mixed state. The bounce-averaged distribution obtained from test-particle simulations cannot be directly used to estimate precipitation because only the loss-cone particles that have left the wave field (MLAT > 35°) are certain to reach the atmosphere. However, since the electrons with pitch angles $\alpha_{eq} < 90°$ interact with parallel-propagating waves in the southern hemisphere, the quarter-bounce averages over the Northern hemisphere in Figures 6d–6f should show a full loss cone, given the high wave amplitudes. Instead, this is the case only with the shortest period $T_{rep} = 0.2$ s, despite the average wave power being kept constant across all simulations. This behavior has a simple origin: when there are large temporal gaps between neighboring elements, some particles miss the wave field entirely and do not get scattered into the loss cone. As a consequence, wave models using long-term averages (e.g., D. Wang et al. (2019)) may predict higher loss rates, especially on the dayside, where trains of chorus elements with longer repetition periods are more common (Shue et al., 2015).

Lastly, we need to discuss the discrepancy in the acceleration time scales predicted by nonlinear and quasilinear models. While our simulation shows the emergence of a significant ultrarelativistic population within less than 10 min, quasilinear calculations predict similar acceleration on the scales of hours and days, which is more in line with spacecraft observations (Horne et al., 2005; Thorne et al., 2013). One reason might be the longitudinal distribution of chorus — with high-amplitude waves limited to a small interval of local times, the ultrarelativistic electrons will experience nonlinear acceleration only during a fraction of their drift period. However, the nonlinear simulations with longitudinal dependence performed by Hsieh et al. (2022) show that the acceleration could still happen on the order of tens of minutes. Another possible reason for the quick build-up of the ultrarelativistic population in our model is therefore the lack of other types of waves. As suggested by Ni et al. (2015) and Drozdov et al. (2020), based on quasilinear simulations, the EMIC emissions drive the loss of high-energy electrons and remove the ultrarelativistic populations from the outer radiation belt. To accurately capture the global evolution of radiation belt electrons during geomagnetically active conditions, we should develop models that include nonlinear scattering driven by both chorus waves and EMIC waves.

Data Availability Statement

The numerical wave model and the test-particle simulation with Liouville mapping were written in Python and are available, including input files, in Hanzelka (2024).

Acknowledgments
MH is supported by the Alexander von Humboldt Postdoctoral Research Fellowship. DW acknowledges support from the DFG funded project 520916080–CHORUS WAVES and the ERC Consolidator Grant 101124679–WIRE. OS acknowledges funding from the GACR Grant 25-18095X and from the Czech MEYS Interexcellence II programme through project LUAUS23152. MH thanks Julia Himmelsbach and Mátyás Szabó-Roberts for helpful discussions. Open Access funding enabled and organized by Projekt DEAL.

References

Agapitov, O. V., Mourenas, D., Artemyev, A. V., Mozer, F. S., Hospodarsky, G., Bonnell, J., & Krasnoselskikh, V. (2018). Synthetic empirical chorus wave model from combined van allen probes and cluster statistics. *Journal of Geophysical Research: Space Physics*, *123*(1), 297–314. https://doi.org/10.1002/2017JA024843

Albert, J. M., Artemyev, A., Li, W., Gan, L., & Ma, Q. (2022). Analytical results for phase bunching in the pendulum model of wave-particle interactions. *Frontiers in Astronomy and Space Sciences*, *9*, 971358. https://doi.org/10.3389/fspas.2022.971358

Allanson, O., Elsden, T., Watt, C., & Neukirch, T. (2022). Weak turbulence and quasilinear diffusion for relativistic wave-particle interactions via a Markov approach. *Frontiers in Astronomy and Space Sciences*, *8*(232), 232. https://doi.org/10.3389/fspas.2021.805699

Allanson, O., Watt, C. E. J., Allison, H. J., & Ratcliffe, H. (2021). Electron diffusion and advection during nonlinear interactions with whistler mode waves. *Journal of Geophysical Research: Space Physics*, *126*(5), e28793. https://doi.org/10.1029/2020JA028793

Artemyev, A. V., Mourenas, D., Zhang, X.-J., & Vainchtein, D. (2022). On the incorporation of nonlinear resonant wave-particle interactions into radiation belt models. *Journal of Geophysical Research: Space Physics*, *127*(9), e2022JA030853. https://doi.org/10.1029/2022JA030853

Artemyev, A. V., Neishtadt, A. I., & Vasiliev, A. A. (2020). Mapping for nonlinear electron interaction with whistler-mode waves. *Physics of Plasmas*, *27*(4), 042902. https://doi.org/10.1063/1.5144477

Baker, D. N. (2021). Wave-particle interaction effects in the Van Allen belts. *Earth Planets and Space*, *73*(1), 189. https://doi.org/10.1186/s40623-021-01508-y

Bell, T. F. (1984). The nonlinear gyroresonance interaction between energetic electron and coherent VLF waves propagating at an arbitrary angle with respect to the earth's magnetic field. *Journal of Geophysical Research*, *89*(A2), 905–918. https://doi.org/10.1029/JA089iA02p00905

Beutier, T., & Boscher, D. (1995). A three-dimensional analysis of the electron radiation belt by the Salammbô code. *Journal of Geophysical Research*, *100*(A8), 14853–14861. https://doi.org/10.1029/94JA03066

Bortnik, J., Thorne, R. M., & Inan, U. S. (2008). Nonlinear interaction of energetic electrons with large amplitude chorus. *Geophysical Research Letters*, *35*(21), L21102. https://doi.org/10.1029/2008GL035500

Chen, H., Wang, X., Chen, L., Zhang, X.-J., Omura, Y., Chen, R., et al. (2024). Nonlinear electron trapping through cyclotron resonance in the formation of chorus subpackets. *Geophysical Research Letters*, *51*(11), e2024GL109481. https://doi.org/10.1029/2024GL109481

Chen, L., Thorne, R. M., Bortnik, J., & Zhang, X.-J. (2016). Nonresonant interactions of electromagnetic ion cyclotron waves with relativistic electrons. *Journal of Geophysical Research: Space Physics*, *121*(10), 9913–9925. https://doi.org/10.1002/2016JA022813

Chen, L., Zhang, X.-J., Artemyev, A., Angelopoulos, V., Tsai, E., Wilkins, C., & Horne, R. B. (2022). Ducted chorus waves cause sub-relativistic and relativistic electron microbursts. *Geophysical Research Letters*, *49*(5), e2021GL097559. https://doi.org/10.1029/2021GL097559

Chen, L., Zhang, X.-J., Artemyev, A., Zheng, L., Xia, Z., Breneman, A. W., & Horne, R. B. (2021). Electron microbursts induced by nonducted chorus waves. *Frontiers in Astronomy and Space Sciences*, *8*, 745927. https://doi.org/10.3389/fspas.2021.745927

Crabtree, C., Tejero, E., Ganguli, G., Hospodarsky, G. B., & Kletzing, C. A. (2017). Bayesian spectral analysis of chorus subelements from the Van Allen Probes. *Journal of Geophysical Research: Space Physics*, *122*(6), 6088–6106. https://doi.org/10.1002/2016JA023547

Denton, R. E., Goldstein, J., Menietti, J. D., & Young, S. L. (2002). Magnetospheric electron density model inferred from Polar plasma wave data. *Journal of Geophysical Research*, *107*(A11), 1386. https://doi.org/10.1029/2001JA009136

Drozdov, A. Y., Usanova, M. E., Hudson, M. K., Allison, H. J., & Shprits, Y. Y. (2020). The role of hiss, chorus, and EMIC waves in the modeling of the dynamics of the multi-MeV radiation belt electrons. *Journal of Geophysical Research: Space Physics*, *125*(9), e2020JA028282. https://doi.org/10.1029/2020JA028282

Foster, J. C., Erickson, P. J., & Omura, Y. (2021). Subpacket structure in strong VLF chorus rising tones: Characteristics and consequences for relativistic electron acceleration. *Earth Planets and Space*, *73*(1), 140. https://doi.org/10.1186/s40623-021-01467-4

Friedel, R., Reeves, G., & Obara, T. (2002). Relativistic electron dynamics in the inner magnetosphere — A review. *Journal of Atmospheric and Solar-Terrestrial Physics*, *64*(2), 265–282. https://doi.org/10.1016/S1364-6826(01)00088-8

Furuya, N., Omura, Y., & Summers, D. (2008). Relativistic turning acceleration of radiation belt electrons by whistler mode chorus. *Journal of Geophysical Research*, *113*(A4), 2007JA012478. https://doi.org/10.1029/2007JA012478

Gan, L., Li, W., Hanzelka, M., Ma, Q., Albert, J. M., & Artemyev, A. V. (2023). Electron precipitation caused by intense whistler-mode waves: Combined effects of anomalous scattering and phase bunching. *Frontiers in Astronomy and Space Sciences*, *10*, 1322934. https://doi.org/10.3389/fspas.2023.1322934

Gao, X., Li, W., Thorne, R. M., Bortnik, J., Angelopoulos, V., Lu, Q., et al. (2014). Statistical results describing the bandwidth and coherence coefficient of whistler mode waves using THEMIS waveform data. *Journal of Geophysical Research: Space Physics*, *119*(11), 8992–9003. https://doi.org/10.1002/2014JA020158

Glauert, S. A., & Horne, R. B. (2005). Calculation of pitch angle and energy diffusion coefficients with the PADIE code. *Journal of Geophysical Research*, *110*(A4), A04206. https://doi.org/10.1029/2004JA010851

Glauert, S. A., Horne, R. B., & Meredith, N. P. (2014). Three-dimensional electron radiation belt simulations using the BAS Radiation Belt Model with new diffusion models for chorus, plasmaspheric hiss, and lightning-generated whistlers. *Journal of Geophysical Research: Space Physics*, *119*(1), 268–289. https://doi.org/10.1002/2013JA019281

Grach, V. S., & Demekhov, A. G. (2020). Precipitation of relativistic electrons under resonant interaction with electromagnetic ion cyclotron wave packets. *Journal of Geophysical Research: Space Physics*, *125*(2), e27358. https://doi.org/10.1029/2019JA027358

Hanzelka, M. (2024). Effects of fine spectral structure of chorus emissions on nonlinear scattering and acceleration of radiation belt electrons: Numerical simulation code [Software]. *Figshare*. https://doi.org/10.6084/M9.FIGSHARE.27124494

Hanzelka, M., Li, W., & Ma, Q. (2023). Parametric analysis of pitch angle scattering and losses of relativistic electrons by oblique EMIC waves. *Frontiers in Astronomy and Space Sciences*, *10*, 1163515. https://doi.org/10.3389/fspas.2023.1163515

Hanzelka, M., & Santolík, O. (2019). Effects of ducting on whistler mode chorus or exohiss in the outer radiation belt. *Geophysical Research Letters*, *46*(11), 5735–5745. https://doi.org/10.1029/2019GL083115

Hanzelka, M., Santolík, O., Omura, Y., & Kolmašová, I. (2021). Measurability of the nonlinear response of electron distribution function to chorus emissions in the earth's radiation belt. *Journal of Geophysical Research: Space Physics*, *126*(9), e29624. https://doi.org/10.1029/2021JA029624

Hanzelka, M., Santolík, O., Omura, Y., Kolmašová, I., & Kletzing, C. A. (2020). A model of the subpacket structure of rising tone chorus emissions. *Journal of Geophysical Research: Space Physics*, *125*(8), e28094. https://doi.org/10.1029/2020JA028094

Hikishima, M., & Omura, Y. (2012). Particle simulations of whistler-mode rising-tone emissions triggered by waves with different amplitudes. *Journal of Geophysical Research*, *117*(A4), A04226. https://doi.org/10.1029/2011JA017428

Hiraga, R., & Omura, Y. (2020). Acceleration mechanism of radiation belt electrons through interaction with multi-subpacket chorus waves. *Earth Planets and Space*, *72*(1), 21. https://doi.org/10.1186/s40623-020-1134-3

Horne, R. B., Thorne, R. M., Glauert, S. A., Albert, J. M., Meredith, N. P., & Anderson, R. R. (2005). Timescale for radiation belt electron acceleration by whistler mode chorus waves. *Journal of Geophysical Research*, *110*(A3), A03225. https://doi.org/10.1029/2004JA010811

Hsieh, Y.-K., Kubota, Y., & Omura, Y. (2020). Nonlinear evolution of radiation belt electron fluxes interacting with oblique whistler mode chorus emissions. *Journal of Geophysical Research: Space Physics*, *125*(2), e2019JA027465. https://doi.org/10.1029/2019JA027465

Hsieh, Y.-K., Omura, Y., & Kubota, Y. (2022). Energetic electron precipitation induced by oblique whistler mode chorus emissions. *Journal of Geophysical Research: Space Physics*, *127*(1), e29583. https://doi.org/10.1029/2021JA029583

Kang, N., Artemyev, A. V., Bortnik, J., Zhang, X.-J., & Angelopoulos, V. (2024). The principal role of chorus ducting for night-side relativistic electron precipitation. *Geophysical Research Letters*, *51*(17), e2024GL110365. https://doi.org/10.1029/2024GL110365

Kennel, C. F., & Engelmann, F. (1966). Velocity space diffusion from weak plasma turbulence in a magnetic field. *Physics of Fluids*, *9*(12), 2377–2388. https://doi.org/10.1063/1.1761629

Kondrashov, D., Drozdov, A. Y., & Shprits, Y. (2024). Nonlinear wave-particle interaction effects on radiation belt electron dynamics in 9 October 2012 storm. *Journal of Geophysical Research: Space Physics*, *129*(9), e2024JA032898. https://doi.org/10.1029/2024ja032898

Kubota, Y., & Omura, Y. (2018). Nonlinear dynamics of radiation belt electrons interacting with chorus emissions localized in longitude. *Journal of Geophysical Research: Space Physics*, *123*(6), 4835–4857. https://doi.org/10.1029/2017JA025050

Kubota, Y., Omura, Y., Kletzing, C., & Reeves, G. (2018). Generation process of large-amplitude upper band chorus emissions observed by Van Allen Probes. *Journal of Geophysical Research: Space Physics*, *123*(5), 3704–3713. https://doi.org/10.1029/2017JA024782

Lemons, D. S., Liu, K., Winske, D., & Gary, S. P. (2009). Stochastic analysis of pitch angle scattering of charged particles by transverse magnetic waves. *Physics of Plasmas*, *16*(11), 112306. https://doi.org/10.1063/1.3264738

Li, W., & Hudson, M. K. (2019). Earth's van allen radiation belts: From discovery to the van allen probes era. *Journal of Geophysical Research: Space Physics*, *124*(11), 8319–8351. https://doi.org/10.1029/2018JA025940

Li, W., Ma, Q., Thorne, R. M., Bortnik, J., Zhang, X.-J., Li, J., et al. (2016). Radiation belt electron acceleration during the 17 March 2015 geomagnetic storm: Observations and simulations. *Journal of Geophysical Research: Space Physics*, *121*(6), 5520–5536. https://doi.org/10.1002/2016JA022400

Li, W., Santolik, O., Bortnik, J., Thorne, R. M., Kletzing, C. A., Kurth, W. S., & Hospodarsky, G. B. (2016). New chorus wave properties near the equator from Van Allen Probes wave observations. *Geophysical Research Letters*, *43*(10), 4725–4735. https://doi.org/10.1002/2016GL068780

Li, W., Thorne, R. M., Bortnik, J., Shprits, Y. Y., Nishimura, Y., Angelopoulos, V., et al. (2011). Typical properties of rising and falling tone chorus waves. *Geophysical Research Letters*, *38*(14), L14103. https://doi.org/10.1029/2011GL047925

Lukin, A. S., Artemyev, A. V., Zhang, X.-J., Allanson, O., & Tao, X. (2024). On the two approaches to incorporate wave-particle resonant effects into global test particle simulations. *Journal of Geophysical Research: Space Physics*, *129*(2), e2023JA032163. https://doi.org/10.1029/2023JA032163

Lyons, L. R. (1974). General relations for resonant particle diffusion in pitch angle and energy. *Journal of Plasma Physics*, *12*(1), 45–49. https://doi.org/10.1017/S0022377800024910

Meredith, N. P., Horne, R. B., Sicard-Piet, A., Boscher, D., Yearby, K. H., Li, W., & Thorne, R. M. (2012). Global model of lower band and upper band chorus from multiple satellite observations. *Journal of Geophysical Research*, *117*(A10), 2012JA017978. https://doi.org/10.1029/2012JA017978

Ni, B., Cao, X., Zou, Z., Zhou, C., Gu, X., Bortnik, J., et al. (2015). Resonant scattering of outer zone relativistic electrons by multiband EMIC waves and resultant electron loss time scales. *Journal of Geophysical Research: Space Physics*, *120*(9), 7357–7373. https://doi.org/10.1002/2015JA021466

Nogi, T., Nakamura, S., & Omura, Y. (2020). Full particle simulation of whistler-mode triggered falling-tone emissions in the magnetosphere. *Journal of Geophysical Research: Space Physics*, *125*(10), e2020JA027953. https://doi.org/10.1029/2020JA027953

Nunn, D., & Omura, Y. (2015). A computational and theoretical investigation of nonlinear wave-particle interactions in oblique whistlers. *Journal of Geophysical Research: Space Physics*, *120*(4), 2890–2911. https://doi.org/10.1002/2014JA020898

Omura, Y., Hikishima, M., Katoh, Y., Summers, D., & Yagitani, S. (2009). Nonlinear mechanisms of lower-band and upper-band VLF chorus emissions in the magnetosphere. *Journal of Geophysical Research*, *114*(A7), A07217. https://doi.org/10.1029/2009JA014206

Omura, Y., Hsieh, Y.-K., Foster, J. C., Erickson, P. J., Kletzing, C. A., & Baker, D. N. (2019). Cyclotron acceleration of relativistic electrons through Landau resonance with obliquely propagating whistler-mode chorus emissions. *Journal of Geophysical Research: Space Physics*, *124*(4), 2795–2810. https://doi.org/10.1029/2018JA026374

Omura, Y., Miyashita, Y., Yoshikawa, M., Summers, D., Hikishima, M., Ebihara, Y., & Kubota, Y. (2015). Formation process of relativistic electron flux through interaction with chorus emissions in the Earth's inner magnetosphere. *Journal of Geophysical Research: Space Physics*, *120*(11), 9545–9562. https://doi.org/10.1002/2015JA021563

Omura, Y., Nakamura, S., Kletzing, C. A., Summers, D., & Hikishima, M. (2015). Nonlinear wave growth theory of coherent hiss emissions in the plasmasphere. *Journal of Geophysical Research: Space Physics*, *120*(9), 7642–7657. https://doi.org/10.1002/2015JA021520

Omura, Y., Nunn, D., & Summers, D. (2013). Generation processes of whistler mode chorus emissions: Current status of nonlinear wave growth theory. In *Dynamics of the earth's radiation belts and inner magnetosphere* (pp. 243–254). American Geophysical Union (AGU). https://doi.org/10.1029/2012GM001347

Omura, Y., & Summers, D. (2006). Dynamics of high-energy electrons interacting with whistler mode chorus emissions in the magnetosphere. *Journal of Geophysical Research*, *111*(A9), A09222. https://doi.org/10.1029/2006JA011600

Orlova, K., & Shprits, Y. (2014). Model of lifetimes of the outer radiation belt electrons in a realistic magnetic field using realistic chorus wave parameters. *Journal of Geophysical Research: Space Physics*, *119*(2), 770–780. https://doi.org/10.1002/2013JA019596

Reeves, G. D., Chen, Y., Cunningham, G. S., Friedel, R. W. H., Henderson, M. G., Jordanova, V. K., et al. (2012). Dynamic radiation environment assimilation model: Dream. *Space Weather*, *10*(3), 2011SW000729. https://doi.org/10.1029/2011SW000729

Remya, B., Lee, K. H., Lee, L. C., & Tsurutani, B. T. (2016). Polarization of obliquely propagating whistler mode waves based on linear dispersion theory. *Physics of Plasmas*, *23*(12), 122120. https://doi.org/10.1063/1.4972534

Ripoll, J.-F., Claudepierre, S. G., Ukhorskiy, A. Y., Colpitts, C., Li, X., Fennell, J. F., & Crabtree, C. (2020). Particle dynamics in the earth's radiation belts: Review of current Research and open questions. *Journal of Geophysical Research: Space Physics*, *125*(5), e2019JA026735. https://doi.org/10.1029/2019JA026735

Saito, S., & Miyoshi, Y. (2022). Butterfly distribution of relativistic electrons driven by parallel propagating lower band whistler chorus waves. *Geophysical Research Letters*, *49*(12), e2022GL099605. https://doi.org/10.1029/2022GL099605

Santolík, O., Gurnett, D. A., Pickett, J. S., Parrot, M., & Cornilleau-Wehrlin, N. (2003). Spatio-temporal structure of storm-time chorus. *Journal of Geophysical Research*, *108*(A7), 1278. https://doi.org/10.1029/2002JA009791

Santolík, O., Gurnett, D. A., Pickett, J. S., Parrot, M., & Cornilleau-Wehrlin, N. (2004). A microscopic and nanoscopic view of storm-time chorus on 31 March 2001. *Geophysical Research Letters*, *31*(2), L02801. https://doi.org/10.1029/2003GL018757

Santolík, O., Kletzing, C. A., Kurth, W. S., Hospodarsky, G. B., & Bounds, S. R. (2014). Fine structure of large-amplitude chorus wave packets. *Geophysical Research Letters*, *41*(2), 293–299. https://doi.org/10.1002/2013GL058889

Santolík, O., Macúšová, E., Kolmašová, I., Cornilleau-Wehrlin, N., & Conchy, Y. (2014). Propagation of lower-band whistler-mode waves in the outer Van Allen belt: Systematic analysis of 11 years of multi-component data from the Cluster spacecraft. *Geophysical Research Letters*, *41*(8), 2729–2737. https://doi.org/10.1002/2014GL059815

Santolík, O., Parrot, M., & Lefeuvre, F. (2003). Singular value decomposition methods for wave propagation analysis. *Radio Science*, *38*(1), 1010. https://doi.org/10.1029/2000RS002523

Santolík, O., Shprits, Y., Kolmašová, I., Wang, D., Taubenschuss, U., Turčičová, M., & Hanzelka, M. (2024). Strong effects of chorus waves on radiation belts expected for future magnetic superstorms. *AGU Advances*, *5*(5), e2024AV001234. https://doi.org/10.1029/2024AV001234

Shprits, Y. Y., Elkington, S. R., Meredith, N. P., & Subbotin, D. A. (2008). Review of modeling of losses and sources of relativistic electrons in the outer radiation belt I: Radial transport. *Journal of Atmospheric and Solar-Terrestrial Physics*, *70*(14), 1679–1693. https://doi.org/10.1016/j.jastp.2008.06.008

Shprits, Y. Y., Subbotin, D. A., Meredith, N. P., & Elkington, S. R. (2008). Review of modeling of losses and sources of relativistic electrons in the outer radiation belt II: Local acceleration and loss. *Journal of Atmospheric and Solar-Terrestrial Physics*, *70*(14), 1694–1713. https://doi.org/10.1016/j.jastp.2008.06.014

Shue, J.-H., Hsieh, Y.-K., Tam, S. W. Y., Wang, K., Fu, H. S., Bortnik, J., et al. (2015). Local time distributions of repetition periods for rising tone lower band chorus waves in the magnetosphere. *Geophysical Research Letters*, *42*(20), 8294–8301. https://doi.org/10.1002/2015GL066107

Stix, T. (1992). *Waves in plasmas*. American Institute of Physics.

Subbotin, D. A., & Shprits, Y. Y. (2009). Three-dimensional modeling of the radiation belts using the Versatile Electron Radiation Belt (VERB) code. *Space Weather*, *7*(10), 2008SW000452. https://doi.org/10.1029/2008SW000452

Subbotin, D. A., Shprits, Y. Y., & Ni, B. (2011). Long-term radiation belt simulation with the VERB 3-D code: Comparison with CRRES observations. *Journal of Geophysical Research*, *116*(A12), A12210. https://doi.org/10.1029/2011JA017019

Summers, D., Omura, Y., Miyashita, Y., & Lee, D.-H. (2012). Nonlinear spatiotemporal evolution of whistler mode chorus waves in Earth's inner magnetosphere. *Journal of Geophysical Research*, *117*(A9), A09206. https://doi.org/10.1029/2012JA017842

Tao, X., Bortnik, J., Albert, J. M., Thorne, R. M., & Li, W. (2014). Effects of discreteness of chorus waves on quasilinear diffusion-based modeling of energetic electron dynamics. *Journal of Geophysical Research: Space Physics*, *119*(11), 8848–8857. https://doi.org/10.1002/2014JA020022

Taubenschuss, U., Khotyaintsev, Y. V., Santolík, O., Vaivads, A., Cully, C. M., Le Contel, O., & Angelopoulos, V. (2014). Wave normal angles of whistler mode chorus rising and falling tones. *Journal of Geophysical Research: Space Physics*, *119*(12), 9567–9578. https://doi.org/10.1002/2014JA020575

Thorne, R. M. (2010). Radiation belt dynamics: The importance of wave-particle interactions. *Geophysical Research Letters*, *37*(22), L22107. https://doi.org/10.1029/2010GL044990

Thorne, R. M., Li, W., Ni, B., Ma, Q., Bortnik, J., Chen, L., et al. (2013). Rapid local acceleration of relativistic radiation-belt electrons by magnetospheric chorus. *Nature*, *504*(7480), 411–414. https://doi.org/10.1038/nature12889

Trakhtengerts, V. Y., Demekhov, A. G., Hobara, Y., & Hayakawa, M. (2003). Phase-bunching effects in triggered VLF emissions: Antenna effect. *Journal of Geophysical Research: Space Physics*, *108*(A4), 1160. https://doi.org/10.1029/2002JA009415

Tsurutani, B. T., & Smith, E. J. (1974). Postmidnight chorus: A substorm phenomenon. *Journal of Geophysical Research*, *79*(1), 118–127. https://doi.org/10.1029/JA079i001p00118

Tu, W., Li, W., Albert, J. M., & Morley, S. K. (2019). Quantitative assessment of radiation belt modeling. *Journal of Geophysical Research: Space Physics*, *124*(2), 898–904. https://doi.org/10.1029/2018JA026414

Varotsou, A., Boscher, D., Bourdarie, S., Horne, R. B., Glauert, S. A., & Meredith, N. P. (2005). Simulation of the outer radiation belt electrons near geosynchronous orbit including both radial diffusion and resonant interaction with Whistler-mode chorus waves. *Geophysical Research Letters*, *32*(19), 2005GL023282. https://doi.org/10.1029/2005GL023282

Volokitin, A., & Krafft, C. (2012). Velocity diffusion in plasma waves excited by electron beams. *Plasma Physics and Controlled Fusion*, *54*(8), 085002. https://doi.org/10.1088/0741-3335/54/8/085002

Wang, D., Shprits, Y. Y., Zhelavskaya, I. S., Agapitov, O. V., Drozdov, A. Y., & Aseev, N. A. (2019). Analytical chorus wave model derived from van allen probe observations. *Journal of Geophysical Research: Space Physics*, *124*(2), 1063–1084. https://doi.org/10.1029/2018JA026183

Wang, G., Su, Z., Zheng, H., Wang, Y., Zhang, M., & Wang, S. (2017). Nonlinear fundamental and harmonic cyclotron resonant scattering of radiation belt ultrarelativistic electrons by oblique monochromatic EMIC waves. *Journal of Geophysical Research: Space Physics*, *122*(2), 1928–1945. https://doi.org/10.1002/2016JA023451

Wong, J.-M., Meredith, N. P., Horne, R. B., Glauert, S. A., & Ross, J. P. J. (2024). New chorus diffusion coefficients for radiation belt modeling. *Journal of Geophysical Research: Space Physics*, *129*(1), e2023JA031607. https://doi.org/10.1029/2023JA031607

Zenitani, S., & Umeda, T. (2018). On the Boris solver in particle-in-cell simulation. *Physics of Plasmas*, *25*(11), 112110. https://doi.org/10.1063/1.5051077

Zhang, X. J., Agapitov, O., Artemyev, A. V., Mourenas, D., Angelopoulos, V., Kurth, W. S., et al. (2020). Phase decoherence within intense chorus wave packets constrains the efficiency of nonlinear resonant electron acceleration. *Geophysical Research Letters*, *47*(20), e89807. https://doi.org/10.1029/2020GL089807

Zhang, X. J., Demekhov, A. G., Katoh, Y., Nunn, D., Tao, X., Mourenas, D., et al. (2021). Fine structure of chorus wave packets: Comparison between observations and wave generation models. *Journal of Geophysical Research: Space Physics*, *126*(8), e29330. https://doi.org/10.1029/2021JA029330

Zheng, L., Chen, L., & Zhu, H. (2019). Modeling energetic electron nonlinear wave-particle interactions with electromagnetic ion cyclotron waves. *Journal of Geophysical Research: Space Physics*, *124*(5), 3436–3453. https://doi.org/10.1029/2018JA026156

References From the Supporting Information

Karpman, V. I., Istomin, I. N., & Shklyar, D. R. (1975). Effects of nonlinear interaction of monochromatic waves with resonant particles in the inhomogeneous plasma. *Physica Scripta*, *11*(5), 278–284. https://doi.org/10.1088/0031-8949/11/5/008

Schulz, M., & Lanzerotti, L. J. (1974). In J. G. Roederer (Ed.), *Particle Diffusion in the Radiation Belts* (Vol. 7). Springer Berlin Heidelberg. https://doi.org/10.1007/978-3-642-65675-0